inter.noise
HAMBURG 2016

Modelling structure-borne sound transmission across a timber-frame wall using SEA

Fabian SCHÖPFER[1,2]; Carl HOPKINS[2]; Andreas R. MAYR[1]; Ulrich SCHANDA[1]

[1] Laboratory for Sound Measurement, University of Applied Sciences Rosenheim, Germany

[2] Acoustics Research Unit, School of Architecture, University of Liverpool, UK.

ABSTRACT

This paper concerns the modelling of sound transmission across a timber-frame wall under mechanical excitation by a point force using Statistical Energy Analysis (SEA). The aim is to develop and experimentally validate a model that would be relevant to machinery such as a heating device or a ventilation system that are often connected to such walls. The prediction is compared against measurements on a wall that forms part of a lightweight test-rig in the Laboratory for Sound Measurement (LaSM) at the University of Applied Sciences Rosenheim. A basic timber frame was built with a single layer of tongue and grooved chipboard on each side of the wall. With this configuration the structure represented a lightweight construction with horizontal junctions in addition to the vertical junctions that are more typical with lightweight constructions formed from plasterboard. A series of SEA models was developed with an increasing degree of complexity regarding the partitioning of the structure into subsystems. Additional experimental work was carried out to determine coupling loss factors across the chipboard joints which were then incorporated in the model. The SEA predictions show reasonable agreement with measured velocities on both leaves and sound pressure levels in the cavities.

Keywords: Statistical Energy Analysis, Lightweight buildings
I-INCE Classification of Subjects Number(s): 43.2.2, 75.2

1. INTRODUCTION

As lightweight building constructions become increasingly more common, there has been increasing interest in the development of prediction models for sound insulation. For lightweight framed walls there are many analytical models for airborne sound transmission – see review in (1). A measurement-based approach has been proposed to allow EN 12354 to be used with lightweight constructions (2, 3) and this is currently being implemented in the ISO and CEN standards. Other approaches are based on empirically determined datasets (e.g. 4). For timber framed walls and floors, Statistical Energy Analysis (SEA) has also been used to model airborne sound transmission (e.g. see 5, 6, 7, 8, 9). For impact sound insulation using the ISO tapping machine on timber joist floors, analytical models have been developed (10) and approaches combining Finite Element Methods (FEM) and SEA (11). For structure-borne sound sources, work by CEN TC126 WG7 has recently focused on quantifying the structure-borne sound power input from building machinery into lightweight structures; hence there is a need for prediction models that can take this measured power input in order to predict sound transmission in timber frame buildings. Previous work on models for structure-borne sound transmission has used predictive SEA to model transmission from one sheet of plasterboard to another across a timber stud (12), and an inverse approach combining FEM and SEA has been proposed for full-size walls (13). For timber frame walls and floors there can be a significant decrease in vibration level across tongue and grooved joints and across successive stud connections (7, 14). This paper investigates the use of SEA to model a timber-frame wall undergoing mechanical point excitation on one side of the wall. The aim is to assess the efficacy of the SEA model against measurements and to assess whether a predictive SEA model could reproduce the decrease in vibration level that occurs with increasing distance from the source plate.

[1] fabian.schoepfer@fh-rosenheim.de

2. TIMBER FRAME WALL CONSTRUCTION

The wall under test is a timber-frame wall which is part of a lightweight test rig at the University of Applied Sciences in Rosenheim. The wall dimensions are shown in Figure 1. The construction is a typical timber framework comprising studs with a separation of 62.5 cm and a cross bar at the bottom and top of the wall. In between the studs there were no cross bars and the cavities were empty (i.e. no mineral wool). On each side of the frame, boards of 19 mm tongue and grooved chipboard were screwed to the timber studs. The boards were arranged such that the longer dimension of the board was perpendicular to the vertical studs. Hence there are horizontal junctions in addition to the vertical junctions that occur with plasterboard walls. Some of these occur above the studs and some in bays; the latter leads to situations where two chipboard plates span a single cavity.

3. EXPERIMENTAL WORK

Prior to the development of the SEA model experimental investigations were carried out in the laboratory. These incorporated measurements on the timber-frame wall to collect data to validate the results of the SEA model. Input data such as material properties were determined as described in (15). The coupling loss factor across the tongue and groove joint between two connected pieces of chipboard was determined experimentally.

3.1 Power input

An electrodynamic shaker was attached at a single point in a bay - see Figure 1. The excitation signal was white noise driven at a sufficient level to ensure sufficient signal-to-noise ratios at all positions used for velocity and sound pressure measurements. The power input was measured using a force transducer and a pair of accelerometers next to the excitation point as shown in Figure 1. The power input was calculated from the average of the two cross-spectra determined from the force signal and accelerometers 1 and 2 respectively.

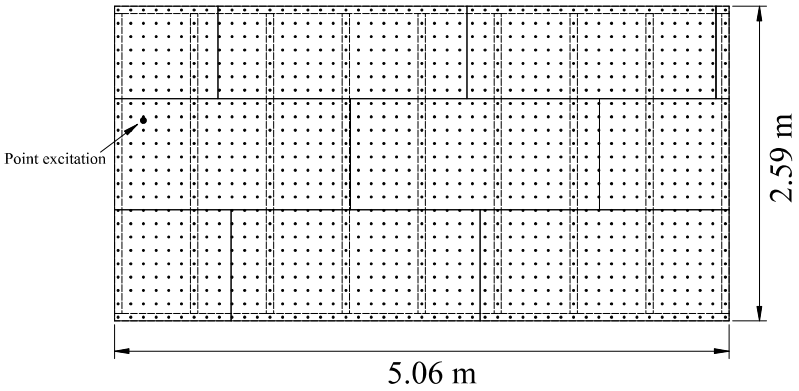

Figure 1 – Measurement grid and excitation point

3.2 Velocity measurements

The vibrational response of the wall was measured at the intersection points of a regular grid on both sides of the wall as sketched in Figure 1 for the source surface. In total 49 x 24 positions were measured for this point excitation on both surfaces. The response was measured with a set of accelerometers being moved across the wall in a series of single measurements. This allowed an investigation of the vibrational behavior of the wall as described in (15) and (16). To compare the measured data with the SEA model, the temporal and spatial average velocities were converted to energy according to equation (1). Where m is the mass of the regarded structure and v is the velocity.

$$E = m\left\langle v^2 \right\rangle_{t,s} \tag{1}$$

3.3 Cavity sound pressure levels

The sound pressure levels were measured inside the cavities of the wall using the same excitation point and signal as used for the velocity measurements. Three holes were drilled through the chipboard sheathing in each bay to insert microphones inside the cavities. The holes were sufficiently large to ensure that there was no contact between the chipboard plates and the microphones. At the entrance point the gap around the microphone was sealed with resilient material. The spatial mean-square sound pressure was converted to energy using equation (2). Where p is the sound pressure, V is the volume of the regarded space, ρ_0 is the density of air and c_0 the phase velocity of sound in air.

$$E = \frac{\left\langle p^2 \right\rangle_{t,s} V}{\rho_0 c_0^2} \tag{2}$$

3.4 Cavity reverberation times

The total loss factor of empty cavities was determined from measurements of the reverberation time. Microphones were inserted into the cavity as described in Section 3.3. A small active speaker that fitted in the narrow cavity was inserted to produce the sound field in the cavity. Most cavities inside building structures (7, 17) often have short reverberation times; hence it was necessary to use reverse-filter analysis to avoid the effect of the filters. These measurements used swept sine excitation with reverse-filter analysis.

3.5 Coupling loss factor between chipboard plates across a tongue and groove joint

A specific characteristic of the structure is the tongue and groove joint that connects the chipboard plates as shown in Figure 2.

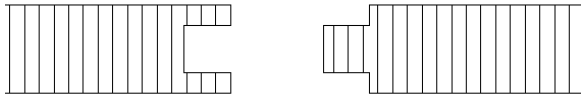

Figure 2 – Tongue and groove joint

No suitable model was available to predict the coupling loss factor for bending wave transmission across a tongue and groove joint; hence it was determined experimentally. Two chipboard plates (as used to build the wall) were freely suspended and connected along one edge. One plate was excited with a shaker at sufficient distance from the junction to avoid significant direct field (more than 1.2 m which is above the reverberation distance up to 5 kHz). On both plates the response was measured with twelve accelerometers randomly distributed away from the direct field of the shaker and the boundaries. This is similar to the procedure used to determine the velocity level differences for the calculation of K_{ij} as described in ISO 10848 (18). To avoid possible airborne flanking between the plates they were shielded with mineral fibre batts (although these were not in contact with the plates). The coupling loss factor was determined from the ratio of the energies (E_j and E_i) on each plate according to equation (3).

$$\eta_{ij} = \frac{E_j}{E_i} \eta_{tot,j} \tag{3}$$

The total loss factor of the freely suspended plate, $\eta_{tot,j}$ was determined by measuring the structural reverberation time in the same configuration with the shaker attached to the coupled receiving plate.

4. SEA Model

Figure 3 schematically indicates the components of the coupled room and wall along with the point force applied on one side of the wall. One possibility to create the SEA model is to divide this system into at least six main subsystems: (a) The shielding on the source side of the wall, (b) the framework, (c) the cavities, (d) the shielding on the receiving side, (e) the receiving room and (f) the source room. However the findings of the experimental investigations on the vibrational behavior showed that there

is a significant decrease of vibrational energy with successive bays and across the tongue and groove joints (15) and (16). Hence each building component (i.e. stud, board) was treated as a single subsystem in the SEA model.

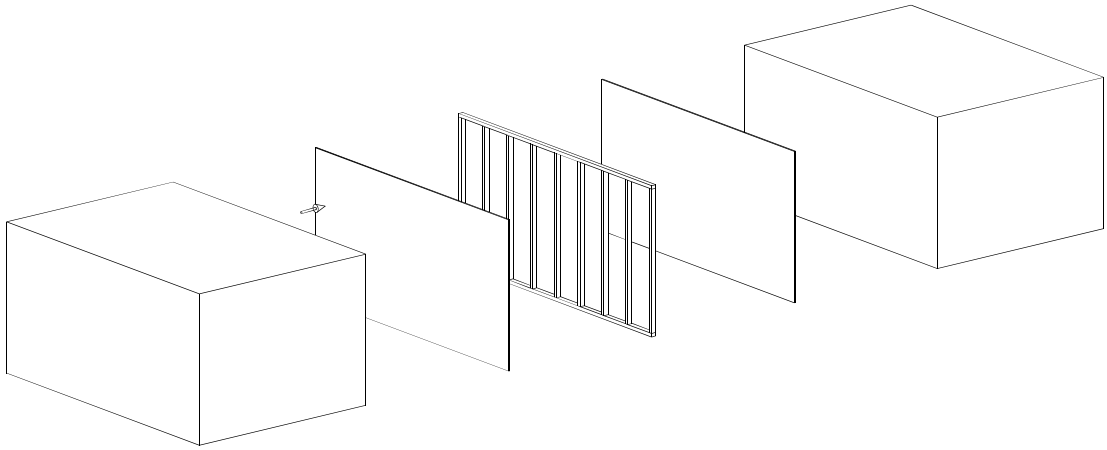

Figure 3 – Schematical sketch of coupled rooms and the wall construction. The arrow indicates the position of the point excitation.

4.1 SEA Subsystems

On the surface where the point force is applied, ten boards (these were different dimensions as this would occur in a real construction) are screwed to the framework. These boards are arranged horizontally as shown in top left sketch in Figure 4. The framework consists of nine studs and a cross bar at the top and the bottom of the wall – see upper right sketch in Figure 4. Together with the chipboard, the framework forms eight cavities – see lower left sketch in Figure 4. On the "receiving surface" of the wall there are also ten boards (different dimensions) screwed to the framework, and the arrangement of these boards differs from the "source surface" – see lower right sketch in Figure 4. The two rooms are considered as individual subsystems. This leads to 41 subsystems in total. Equation (4) gives the power balance equations for this particular system.

$$\begin{bmatrix} \eta_1 & -\eta_{12} & \cdots & -\eta_{411} \\ -\eta_{12} & \eta_2 & & \\ \vdots & & \ddots & \\ -\eta_{141} & & & \eta_{41} \end{bmatrix} \begin{bmatrix} E_1 \\ E_2 \\ \vdots \\ E_{41} \end{bmatrix} = \begin{bmatrix} 0 \\ W_{in,2} / \omega \\ \vdots \\ 0 \end{bmatrix} \tag{4}$$

Where η_{ij} is the coupling loss factor from subsystem i to j, η_i is the total loss factor for subsystem i (equation (5)), E_i is the energy in subsystem i and $W_{in,2}$ is the power input in subsystem 2 (see figure 4, position of point excitation).

$$\eta_i = \eta_{\text{int},i} + \sum_{j=1}^{J} \eta_{ij} \tag{5}$$

The SEA model is shown in Figure 5 in a simplified format where the same type of subsystem is grouped together. For clarity, the power transmissions W_{ij} were not included above the arrows in this sketch. W_d indicates the dissipated power and $W_{in,2}$ the power input in subsystem 2. Although the power input arrow is sketched towards the whole group of source surface boards it only applies to subsystem 2 as it can be seen in figure 4.

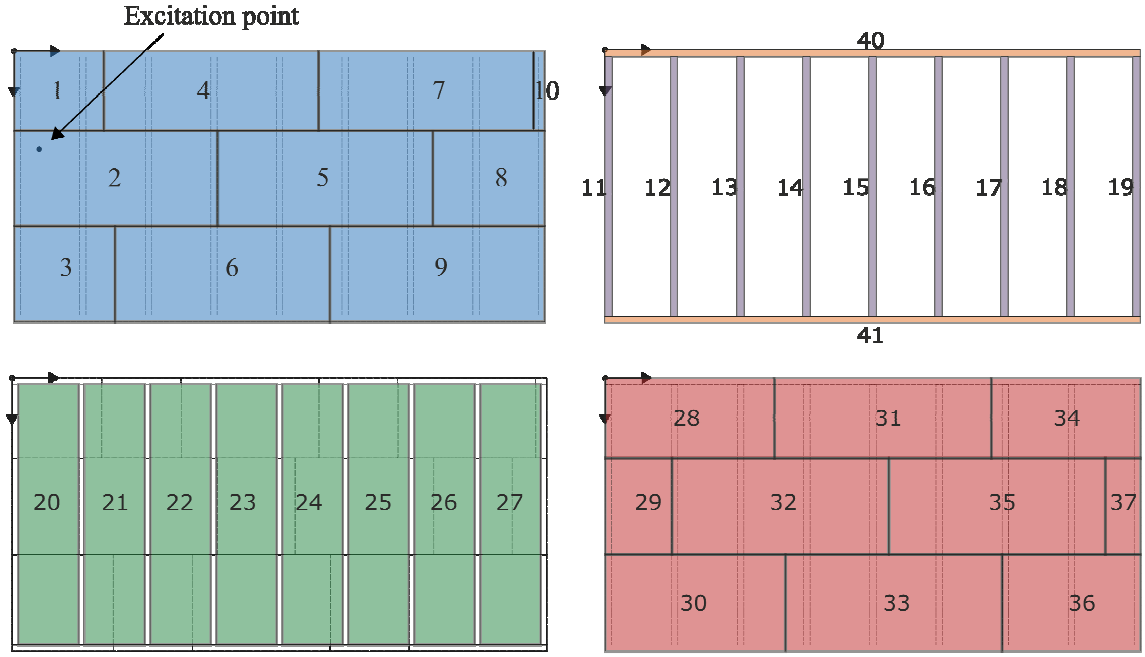

Figure 4 – Sketch indicating the subsystems (top left: boards on the source surface including the position of the excitation point; top right: timber studs and cross bars; bottom left: cavities; bottom right: boards on the receiving surface)

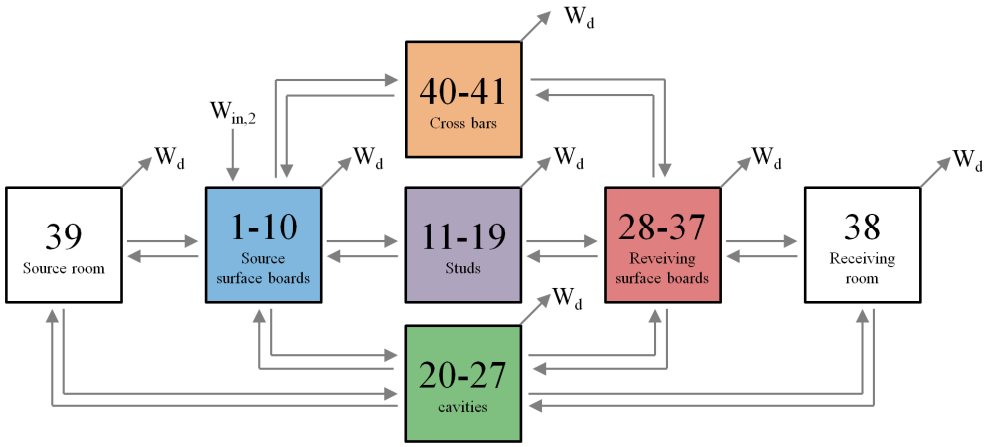

Figure 5 – SEA Model

4.2 Assumptions

All the coupling loss factors that were used in the model were predicted except the plate coupling which was measured as described above. The internal loss factors for the chipboard and the timber were measured as described in (15). The internal loss factor in the empty cavities was modelled according to Price and Crocker (19) with an estimated absorption coefficient for the cavity perimeter.

The coupling between plates and the framework was modelled as a point connection for every screw using infinite and semi-infinite plate and beam mobilities as an approximation. The screws were considered as a rigid connection (7). As shown in Figure 4 each cavity is covered with a number of fractional surface areas of the boards. The coupling between the cavities and the boards was modelled using the fractional area facing the cavity as a factor for the energy radiated from each plate into a cavity. The radiation was modelled according to Leppington's approach for thin, rectangular, isotropic finite plates (20). The sound field in the cavities was modelled as a one-dimensional field below the first tangential mode. Above the first cross cavity mode the sound field was modelled as being

three-dimensional. In between these frequencies a two-dimensional field was assumed. Additional nearfield radiation was applied in the model for the first cavity due to the point force that was applied to the chipboard facing into that cavity. The non-resonant coupling between the cavities and the rooms was modelled in the same way as described in (9) respectively (7).

5. RESULTS

5.1 Coupling loss factor across a tongue and groove joint

The measured coupling loss factor across a tongue and groove joint was averaged from both directions (i→j and j→i) as shown in Figure 6. This shows that with increasing frequency the coupling strength gets weaker. This coupling loss factor was used in the SEA model by normalizing it to the coupling length between specific boards.

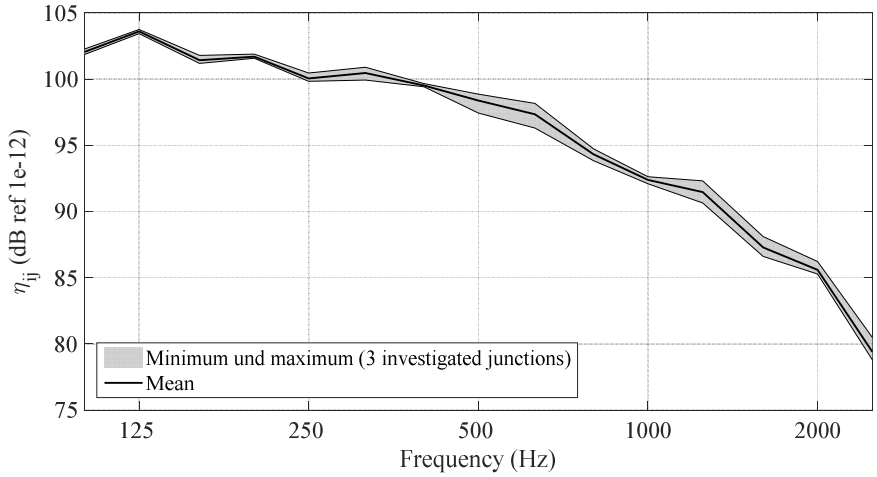

Figure 6 – Measured coupling loss factor across a tongue and groove joint.

5.2 Comparison of measured and SEA total loss factor of the cavity

The measured total loss factor in the cavity can be compared against the set of predicted coupling loss factors and the internal loss factor for a sample cavity. The cavity that is considered is coupled to three boards on the source surface and five boards on the receiving surface as indicated in Figure 7 and there is non-resonant coupling from the cavity to the source and the receiving rooms.

The predicted total loss factor is calculated according to equation (5) and is in reasonable agreement with the measured total loss factor below 250 Hz. In the mid-frequency range between 250 Hz and 1000 Hz the prediction slightly underestimates the loss factor, whereas at higher frequencies at and above 2000 Hz it slightly overestimates; however the general trend is similar.

5.3 Comparison of SEA with measured velocities and sound pressure levels

The solution of equation (4) can be compared to the energies determined from the measured velocities and sound pressures as described in sections 3.2 and 3.3. For the measured velocities the spatial average was calculated for every plate separately omitting points close to the edges and points above studs. Using these spatial average velocities, the energy was determined with the mass of each corresponding plate. For the validation all energies determined in the model and all measured energies were normalized to subsystem 2 where the point force was applied. Using these normalized energies, the level difference between measurement and SEA model was calculated according to equation (6) for each individual subsystem.

$$D_i = 10\lg\frac{E_{i,SEA}}{E_{2,SEA}} - 10\lg\frac{E_{i,meas}}{E_{2,meas}} \tag{6}$$

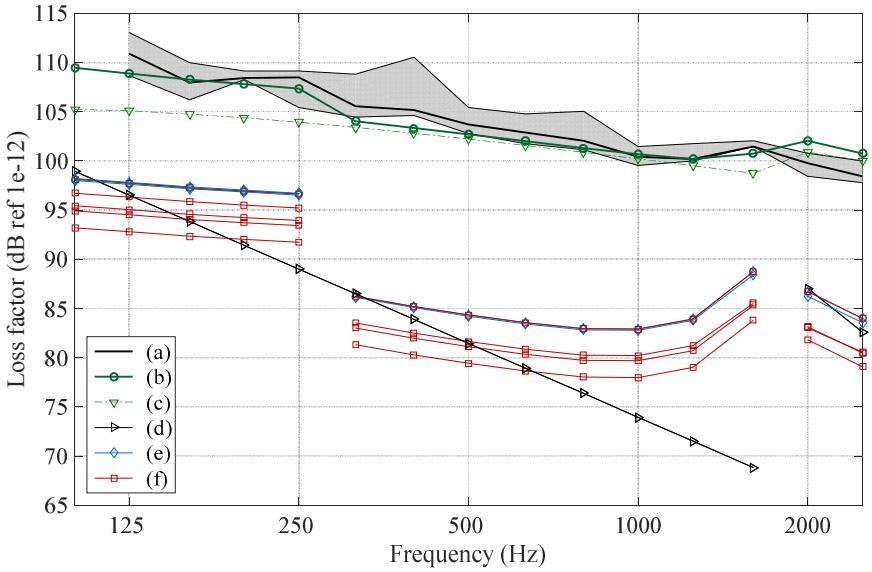

Figure 7 – Comparison of experimentally determined total loss factor of a cavity and the predicted total loss factor for subsystem 22 (see figure 4). (a) Experimentally determined total loss factor (Median with minimum and maximum value), (b) predicted total loss factor according to equation (5), (c) internal loss factor according to (19), (d) coupling between cavities and rooms, (e) coupling between cavity and source room plates and (f) coupling between cavity and receiving room plates

In Figure 8 the difference between the SEA energies and the measured energies is plotted for all boards on the source side of the wall (subsystems 1 to 9 - subsystem 10 is not shown due to its very small dimensions). Subsystem 2 is the plate on which point force excitation was applied. According to equation (6) negative values indicate an underestimation of the SEA model. The same procedure was applied to the measured velocities on the receiving surface (subsystems 28 to 37). The differences between SEA and measurements are shown in Figure 10. Similarly, the measured energy in each cavity (subsystems 20 to 27) is compared with SEA in Figure 9.

The validation for the source surface shows deviations mainly within a 10 dB range with occasional deviations up to 18 dB. Similar findings occurred for the receiving side of the wall where there is reasonable agreement for the plates close to the excitation point. With increasing distance from the excited plate the deviations become larger but typically <10 dB.

The experimentally determined energies in the cavities can only be regarded as a rough estimate since only three microphone positions were used in each cavity. However the results can indicate the validity of the SEA model as the general trend shows reasonable agreement with deviations typically <10 dB.

6. CONCLUSIONS

SEA has been used to model vibration transmission across a timber-frame structure formed from chipboard plates with tongue and grooved connections. The system was divided into 41 subsystems by treating every stud, board and cavity as an individual subsystem. All coupling loss factors in the model were predicted except for measured coupling across the tongue and groove joint. The predicted total loss factor of the cavity showed reasonable agreement with measurements. Measured velocities on the boards and sound pressure inside the cavities were used to assess the SEA model. Considering the assumption in the SEA model, a detailed subdivision of the wall into subsystems gives reasonable agreement with measurements with the smallest errors occurring for subsystems near the source subsystem.

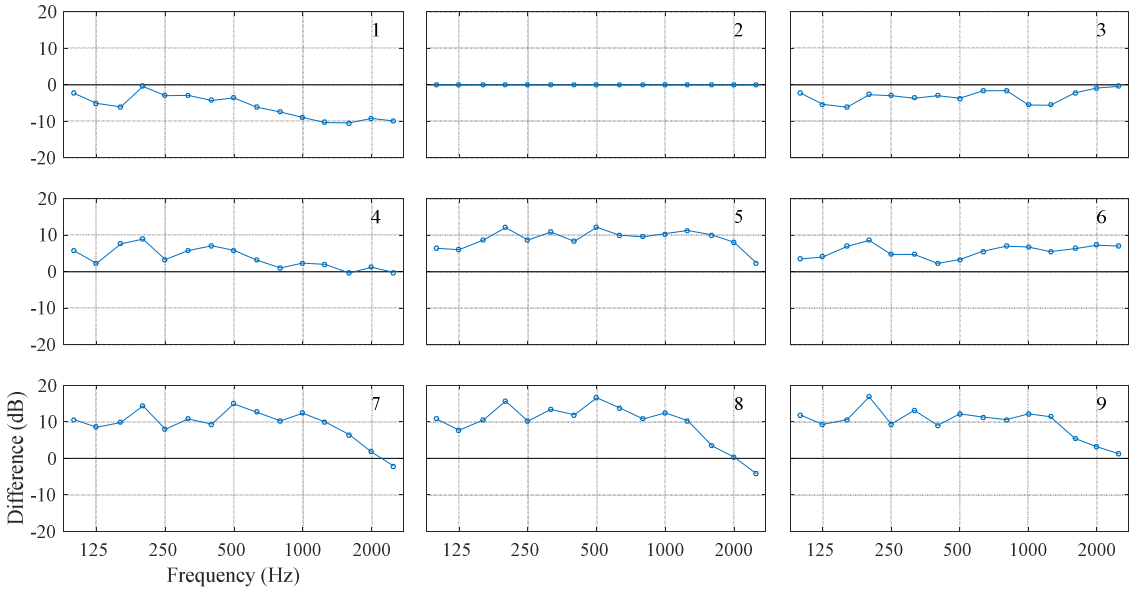

Figure 8 – Difference, *D*, between SEA predicted and measured energy level differences for the plate subsystems on the source surface. The numbers in the corner of the plots indicate the subsystem. Subsystem 10 is not shown due to its very small dimensions.

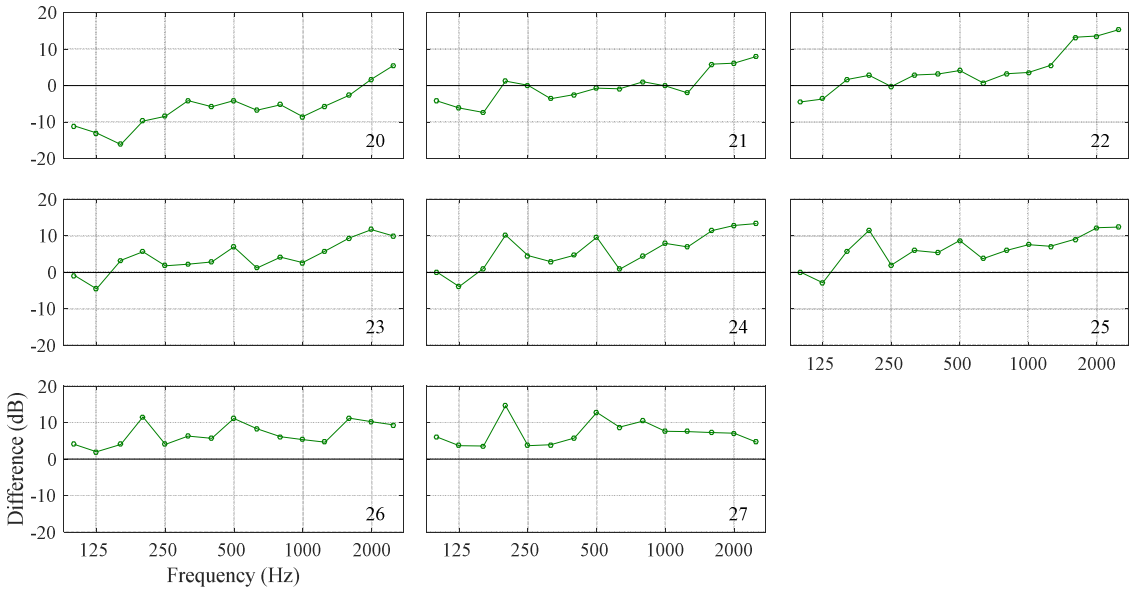

Figure 9 - Difference, *D*, between SEA predicted and measured energy level differences between the source plate and cavity subsystems. The numbers in the corner of the plots indicate the subsystem.

ACKNOWLEDGEMENTS

This work is part of a research project in cooperation with the University of Applied Sciences Stuttgart and the Acoustics Research Unit at the University of Liverpool. It is funded by the German Federal Ministry of Education and Research in the program FHprofUnt (support code: 03FH089PB2). The authors would also like to thank the companies Müller-BBM Vibro Akustik Systeme GmbH for the support in the measurements and Regnauer Fertighaus GmbH for the support in planning and construction of the lightweight test rig.

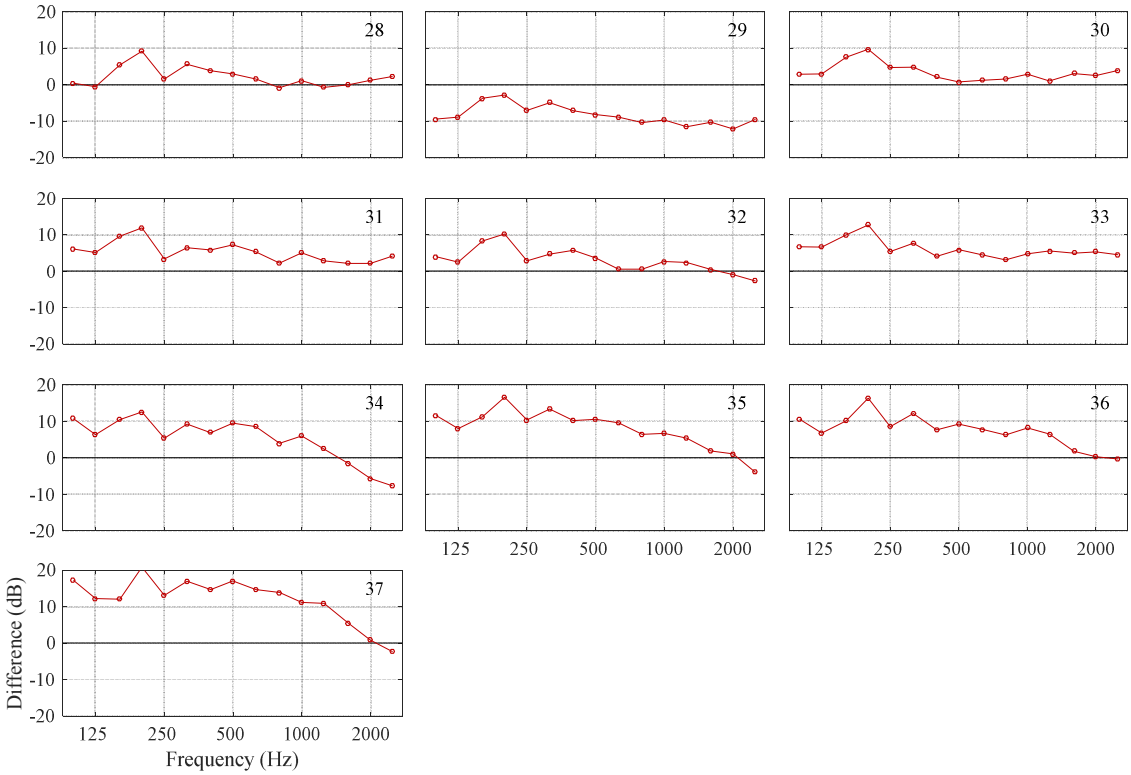

Figure 10 – Difference, *D*, between SEA predicted and measured energy level differences for the plate subsystems on the receiving surface. The numbers in the corner of the plots indicate the subsystem.

REFERENCES

1. Hongisto V. Sound insulation of double panels – comparison of existing prediction models. Acta Acust Acust 2006;92:61-78.
2. Guigou-Carter C, Villot M. Wetta R. Prediction method adapted to wood frame lightweight constructions. Build Acoust 2006;13(3):173-188.
3. Villot M. and Guigou-Carter C. Measurement methods adapted to wood frame lightweight constructions. Build Acoust 2006;13(3):189-198.
4. Arnold J and Kornadt O (2014): Beschreibung Körperschallinduzierter Schalldruckpegel mit Hilfe von Übertragungsfunktionen. In: Nabil A. Fouad (Hg.): Bauphysik Kalender 2014. D-69451 Weinheim, Germany: Wiley-VCH Verlag GmbH, S. 641–663.
5. Craik RJM and Smith RS. Sound transmission through double leaf lightweight partitions. Part I: Airborne sound. Appl Acoust 2000;61:223-245.
6. Craik RJM and Galbrun L. Vibration transmission through a frame typical of timber-framed buildings. J Sound Vib 2005;281:763-782.
7. C. Hopkins. Sound insulation, Butterworth-Heinemann, 2007. ISBN 978-0-7506-6526-1.
8. Schoenwald S. Flanking sound transmission through lightweight framed double leaf walls – Prediction using statistical energy analysis. Eindhoven University of Technology. PhD thesis (2008).
9. Churchill C and Hopkins C. Prediction of airborne sound transmission across a timber-concrete composite floor using Statistical Energy Analysis. Appl Acoust 2016;110:145-159.
10. Brunskog J and Hammer P. Prediction model for the impact sound level of lightweight floors. Acta Acust Acust 2003;89:309-322.
11. Guigou-Carter C and Coguenanff C. Prediction of the acoustic performance of lightweight wood-based floor. Proc Internoise 2015, San Francisco, USA.
12. Craik RJM and Smith RS. Sound transmission through double leaf lightweight partitions. Part I: Airborne sound, Part II Structure-borne sound. Appl Acoust 2000;61:247-269.

13. Kouyoumji J-L, Bard D, Borello G, Guigou C. Challenges for acoustic calculation models in "Silent Timber Build" Part 2. Proc Internoise 2014, Melbourne, Australia.
14. Nightingale TRT and Bosmans I. Vibration response of lightweight wood frame building elements. Build Acoust 1999;6(3/4):269-288.
15. Schöpfer F, Hopkins C, Mayr A, Schanda U (2014): Case study on the vibrational behavior of a timber-frame structure. Proc Forum Acusticum 2014. Krakow, Poland.
16. Schöpfer F, Hopkins C, Mayr A, Schanda U (2015): Structure-borne sound propagation across a double leaf timber-frame wall. Proc 22nd International Congress on Sound and Vibration. Florence, Italy.
17. Hopkins C. Sound transmission across a separating and flanking cavity wall construction. Appl Acoust 1997;52(3/4):259-272.
18. EN ISO 10848-1:2006: Acoustics – Laboratory measurement of the flanking transmission of airborne and impact sound between adjoining rooms – Part 1: Frame document. International Organization for Standardization.
19. Price AJ and Crocker MJ. Sound transmission through double panels using statistical energy analysis. J Acoust Soc Am 1970;47(1/3):683-693.
20. Leppington FG, Broadbent EG, Heron KH, Mead SM. Resonant and non-resonant acoustic properties of elastic panels I. The radiation problem. Proc R Soc London 1986;A406:139-171.